Spatiotemporal Coordination of RPE Cell Quality by Extracellular Vesicle miR-494-3p Via Competitive Interplays With SIRT3 or PTEN

Junji Hamuro,[1] Tomoko Yamashita,[2] Yohei Otsuki,[1] Nao Hiramoto,[1] Mayuka Adachi,[1] Takafumi Miyatani,[1] Hiroshi Tanaka,[1] Morio Ueno,[1] Shigeru Kinoshita,[2] and Chie Sotozono[1]

[1]Department of Ophthalmology, Kyoto Prefectural University of Medicine, Kyoto, Japan
[2]Department of Frontier Medical Science and Technology for Ophthalmology, Kyoto Prefectural University of Medicine, Kyoto, Japan

Correspondence: Junji Hamuro, Department of Ophthalmology, Kyoto Prefectural University of Medicine, 465 Kajii-cho, Hirokoji-agaru, Kawaramachi-dori, Kamigyo-ku 602-0841, Kyoto, Japan; jshimo@koto.kpu-m.ac.jp.

Received: February 2, 2023
Accepted: April 13, 2023
Published: May 10, 2023

Citation: Hamuro J, Yamashita T, Otsuki Y, et al. Spatiotemporal coordination of RPE cell quality by extracellular vesicle miR-494-3p via competitive interplays with SIRT3 or PTEN. *Invest Ophthalmol Vis Sci.* 2023;64(5):9. https://doi.org/10.1167/iovs.64.5.9

Purpose. To reveal the molecular mechanism underlying degeneration in human retinal pigment epithelial (hRPE) cells with dysfunctional mitochondrial homeostasis.

Methods. The expression of recently identified miR-494-3p in extracellular vesicles (EV) released from induced-pluripotential-stem-cell–derived human RPE (iPS-hRPE), during coculture with macrophages (Mps) was investigated in iPS-hRPE and ARPE cells differentiated in the presence of nicotinamide (Nic-ARPE). The expression of phosphatase and tensin homolog (PTEN), sirtuin3 (SIRT3), and mitochondrial marker proteins before and after the transfection of miR-494-3p inhibitor and mimic, and the changes in mitochondrial metabolism, membrane potential, and oxidative phosphorylation (OXPHOS) were monitored.

Results. Compared with senescent dedifferentiated ARPE19 cells, iPS-hRPE and Nic-ARPE cells expressed elevated levels of mitochondrial marker proteins but a repressed cellular miR-494-3p level. The expression of target proteins of miR-494-3p, PTEN, and SIRT3 was upregulated along with the differentiation disposition of these RPE cells. The ratio of PTEN/SIRT3 in de-differentiated ARPE19 cells was surprisingly elevated by around 20 times compared with that in iPS-hRPE and Nic-ARPE cells. The novel molecular interplay of EV miR-494-3p either with mitochondria selective SIRT3 or organelle nonselective PTEN was found to participate in the degeneration of hRPE cells by inducing mitochondrial dysfunctions and repressed OXPHOS, mitochondrial membrane potential, and ATP and NAD^+ production.

Conclusions. Our results demonstrate a clear causal link between miR-494-3p and hRPE cell degeneration via the regulation of mitochondrial integrity. EV miR-494-3p may play a pivotal role in pathogenic spreading of degenerated hRPE cells from the local perifovea throughout the macula.

Keywords: RPE cell quality, miRNA, PTEN, SIRT3, mitochondria

Age-related macular degeneration (AMD) is a leading cause of blindness in elderly persons in developed countries.[1,2] Ocular-infiltrating macrophages (Mps) aggravate the pathogenesis of AMD-associated chronic inflammation.[3–10] Photoreceptors, retinal pigment epithelial (RPE) cells, and the choroid form a functional unit that is required for visual function.[11] RPE tissues form a single layer of highly polarized cells that is located between the photoreceptors and the choroid. In early AMD, RPE cells exhibit mitochondrial dysfunction and constitute cellular heterogeneity with degenerated and nondegenerated RPE cells.[12–14] Our research group and those of others have reported on the epigenetic regulation of the epithelial mesenchymal transition (EMT), a typical form of degeneration, induced in RPE cells by the synergistic action of TNF-α and TGF-β.[15–17] The integrity of RPE tissues will be either further injured or restrained by the expansion of degenerated cell clusters, depending on the exposed paracrine signals provided by ambient microenvironmental niches.

RPE cells cultured with undifferentiated human monocytes can induce an immune-regulatory phenotype.[18] A number of microRNAs (miRs) associated with inflammatory responses have been identified in both Mps and RPE cells; however, miRs associated with exosomes (Exo) or extracellular vesicles (EVs) from human RPE (hRPE) cells have not yet been functionally characterized. In a previous study, we revealed that EVs produced by hRPE cells can trigger a vicious inflammatory cycle to produce MCP-1, IL-6, and IL-8, partially mediated through EV miRs. Microarray analysis of the miRs in EVs revealed a selective increase in the secretion of miR-494-3p in EVs released from induced-pluripotential-stem-cell–derived hRPE (iPS-hRPE) cells during their cellular interplay with Mps.

Studies of the interesting interactions between Mps and RPE cells[19,20] have identified a novel paracrine mode of EV cargo-mediated RPE cell degeneration that extended to neighboring innocent RPE cells in hRPE tissues. Microarray analysis of miRs in EV cargo identified a selective increase of miR-494-3p in EVs released from iPS-hRPE cells during their interplay with Mps.[21,22] In this article, we describe the newly found molecular network regulating RPE mitochondrial functions by miR-494-3p (Supplementary Fig. S1). Considering our recent findings and hypothesis,[22] EV-miR-494-3 may induce the spread of degenerated foci in a single-cell layer of RPE tissues into the neighbors through the regulation of either mitochondria localized sirtuin-3 (SIRT3) or organelle nonselectively distributed phosphatase and tensin homolog (PTEN). A diagram of the general experimental set up would help understand the complex figures (Supplementary Table S1, Supplementary Fig. S2).

Stem-cell–derived RPE cells, such as iPS-hRPE cells, have been found to lose their polarized organization and RPE functions after only a few passages in culture.[23] However, the human RPE cell line ARPE-19 no longer forms a differentiated morphology[24] after two decades of passages. In contrast, nicotinamide (NAM) has been shown to enhance the RPE phenotype and to prevent EMT and senescence in multiple RPE cell model systems.[17,25,26] NAM prevents and reverses the RPE cell EMT that is induced by TGF-β and TNF-α treatment.[17] However, in the absence of NAM in the culture medium, hRPE cell will lose its cobblestone appearance and undergo dedifferentiation.[27] Furthermore, owing to the Japanese government's legal prohibition on the handling of primary hRPE from eye donors, we have been obliged to apply two types of hRPE cells in this study: iPS-hRPE and Nic-ARPE cells (i.e., ARPE19-derived hRPE cells obtained in the presence of NAM).[26,27] The current study may provide insights into the paracrine cellular interplay among heterogeneous RPE cells during diseased perturbations through EV miR-494-3p.

Material and Methods

Reagents

Dulbecco's modified Eagle medium (DMEM), F-12 Ham nutrient mixture, and L-glutamine were purchased from Sigma-Aldrich Corp. (St. Louis, MO, USA); penicillin-streptomycin and B-27 were purchased from Life Technologies, Inc. (Grand Island, NY, USA); RPMI medium 1640 and fetal bovine serum (FBS) were obtained from Gibco Industries Inc. (Thermo Fisher Scientific, Waltham, MA, USA); and plastic culture plates were obtained from Corning (Corning, NY, USA). The serum-free medium for iPS-hRPE culture was DMEM/F-12 (7:3) with 2 mM glutamine supplemented with 1% B-27 and 1% penicillin-streptomycin, and that for Nic-ARPE cells was MEM-Nic (MEM alpha with GlutaMAX; Thermo Fisher Scientific), 1% fetal bovine serum, 100 U/mL penicillin, 100 µg/mL streptomycin, 1% N2 supplement (Thermo Fisher Scientific), taurine (0.25 mg/mL) (Sigma-Aldrich), hydrocortisone (20 ng/mL) (Sigma-Aldrich), triiodothyronine (0.013 ng/mL) (Sigma-Aldrich), and 10 mM NAM (Sigma-Aldrich).[26,27] The media were changed every three days. The culture and passages for iPS-hRPE and Nic-ARPE cells are illustrated in Figure 1.

Antibodies

The primary antibodies used for immunocytochemistry included rabbit anti-zonula occludin (ZO)-1 (617300; Invitrogen, Carlsbad, CA, USA), mouse anti-ZO-1 (339100;

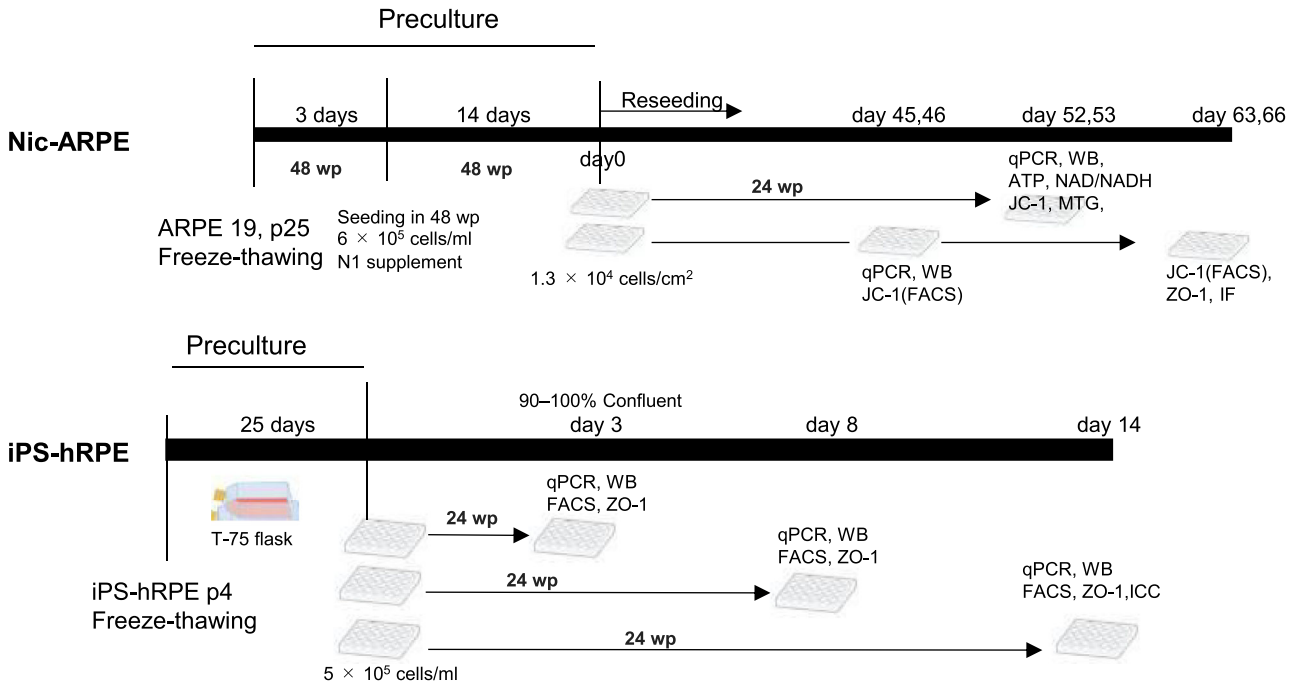

Figure 1. Preparation of Nic-ARPE and iPS-hRPE cell cultures to estimate the culture period required for differentiation disposition. ARPE-19 cell line cultured for three days in DMEM/F12 was reseeded into 48 well plates (wp) with a cell density of 6 × 10^5 cells/ml × 0.25 ml/well in the presence of nicotinamide (NAM, 10mM) for 14 days (preculture). Thereafter, the harvested cells were reseeded into a new wp with a cell density of 1.3 × 10^4 cells/cm^2 in the presence of NAM (10mM) for 45-65 days to gain Nic-ARPE cells for the functional evaluation. iPS-hRPE cells (P3 or P5) were seeded into a wp with a cell density of 5 × 10^5 cells/cm^2 and cultured for 3-14 days. The medium was changed every three days for both cultures.

Investigative Ophthalmology & Visual Science

Invitrogen), mouse anti-cellular retinaldehyde-binding protein (CRALBP; ab15051; Abcam, Cambridge, MA, USA), rabbit anti-paired box 6 (Pax-6; PRB-278P; BioLegend, San Diego, CA, USA), and mouse anti-Bestrophin (BEST)1 (ab2182; Abcam). The secondary antibodies used were goat anti-mouse and goat anti-rabbit IgG conjugated to Alexa Fluor 488, 594, or 647 (Life Technologies). For Western blotting, the antibodies used included rabbit anti-PGC1 alpha (NBP1-04676; Novus Biologicals, Littleton, CO, USA), rabbit anti-b-Actin (CST 4967S; Cell Signaling Technology, Danvers, MA, USA), rabbit anti-PTEN (CST 9552S; Cell Signaling Technology), rabbit anti-SIRT1 (CST 9475; Cell Signaling Technology), rabbit anti-SIRT3 (ab217319; Abcam), rabbit anti-TFAM (CST 8076S; Cell Signaling Technology), mouse anti-TOMM20 (ab56783; Abcam), and mouse anti-VDAC (ab14734; Abcam). The secondary antibodies used were goat anti-mouse IgG and goat anti-rabbit IgG (H+L; Southern Biotech, Birmingham, AL, USA). The details of the antibodies used are listed in Supplementary Table S2.

Cell Culture

ARPE-19 cells were obtained from the American Type Culture Collection (passage 21). ARPE-19 cells were thawed and cultured in DMEM/F12, 10% certified FBS, and 1% penicillin/streptomycin until the culture vessel was 95% to 100% confluent. The media were changed every three days. ARPE-19 cells at passage 24 or 25 and showing the de-differentiated phenotypes (Supplementary Fig. S3), detected by the primers listed in Supplementary Table S3, were used for the experiment. Primary cultures of iPS-cell–derived hRPE (iPS-hRPE) cells, which were originally donated by Prof. Masayo Takahashi, followed the procedures described previously.[28,29] The primary hRPE cells, iPS-hRPE cells were cultured and propagated in serum-free DMEM, seeded at passages 4 to 6 at 1.25 to 1.33 $\times$ 10^5 cells/cm^2 on plastic culture plates (Corning) coated with iMatrix 511 (385-07361; Wako, Osaka, Japan), and grown to 100% confluence as described previously.[22] Briefly, 15 mL of cell suspension was seeded in the medium with a cell density of 1.25 to 1.333 $\times$ 10^5 cells/cm^2 in a T75 flask precoated with Matrigel 511. The passage was limited until the sixth life span to gain mature differentiated phenotypes. The differentiation inclined phenotypes of primary iPS-hRPE cells were evaluated by immunohistochemistry for the expression of microphthalmia-associated transcription factor, ZO-1, RPE65, BEST, and Pax-6. The ARPE-19 cells cultured in media with added NAM (Nic-ARPE) were cultured in MEM-Nic and propagated following the procedures reported by Hazim et al.[26] NAM serves as a precursor for the production of NAD^+, $NADP^+$, and other substrates that participate in metabolic pathways.[30] The typical procedures of the cultures and passage are also illustrated in Figure 1. In all experiments, ARPE-19 cells were used within five additional passages after freeze-thawing the cells from the American Type Culture Collection.

Immunocytochemistry

The collected hRPE cells were washed three times with Dulbecco's phosphate-buffered saline solution (Nacalai Tesque, Kyoto, Japan) before being fixed with cold methanol for 10 minutes at 30°C following the procedures reported previously.[16] Briefly, cell permeabilization was achieved with 0.2% Triton X-100 for 15 minutes at room temperature (RT). The appropriate Alexa Fluor-conjugated secondary antibodies were used for one hour at RT in the dark. Then, fluorescence microscopy imaging was performed (BZ9000; Keyence, Osaka, Japan). The primary antibodies used included ZO-1 (1:500 dilution) (Invitrogen 617300), mouse anti-ZO-1 (1:500 dilution; Invitrogen 339100), mouse anti-CRALBP (1:200 dilution; Abcam ab15051), rabbit anti Pax-6 (1:500 dilution; Biolegend PRB-278P), and mouse anti-BEST1 (1:500 dilution; Abcam ab2182).

Phase Contrast and Fluorescence Microscopy

Phase contrast microscopy and fluorescence microscopy images were obtained using a Keyence fluorescence microscope (BZ9000).

ELISA

The procedures followed our recent publication.[21] Briefly, the culture supernatants (CSs) were harvested after a 48-hour culture period. The ELISA kits for human VEGF, PEDF, MCP-1, IL-8, and IL-6 were obtained from BD Biosciences (San Diego, CA, USA). The measurements were performed in quadruplicate and repeated as three independent experiments. The averages of the quadruplicates are shown (Fig. 2).

RNA Extraction and miRNA Profiling 3D-Gene Microarray Analysis

RNA extraction was performed as described previously.[31] For miR expression profiling, 3D-Gene Human miRNA Oligo Chips (miR Base, version 17-19; Toray Industries, Tokyo, Japan) were used and analyzed as reported previously.[31] All data were globally normalized per microarray such that the median of the signal intensity was adjusted to 25 (Fig. 3).

Quantitative Real-Time Polymerase Chain Reaction

Total RNA was extracted from hRPE cells using the miRNeasy Mini Kit (Qiagen, Hilden, Germany) according to the manufacturer's protocol. The miRNA and gene expressions were normalized to RNU44 or 18S using the comparative cycle threshold method (2^-ΔCT). Primers and probes were purchased from Thermo Fisher Scientific (Supplementary Table S3).

miR Mimics or Inhibitors and a Pharmacological Inhibitor

The transfection of either miR mimics or inhibitors at 50nM was conducted using a DharmaFECT 1 reagent (Horizon Discovery, Cambridge, UK) in accordance with the manufacturer's protocol. The mimics and inhibitors targeting miRNA-494-3p and the negative control (NC) of mimics and inhibitors were purchased from Thermo Fisher Scientific (Supplementary Table S4). The NC inhibitor is a negative control for the inhibitor, which does not show the inhibition of miR-494-3p activity, although it shares with the sequence analogy with the inhibitor. Across experiments, the efficiency of the transduction of either miR mimics or inhibitors was evaluated by the quantitative real-time PCR (qRT-PCR) and normalized to RNU44 using the comparative

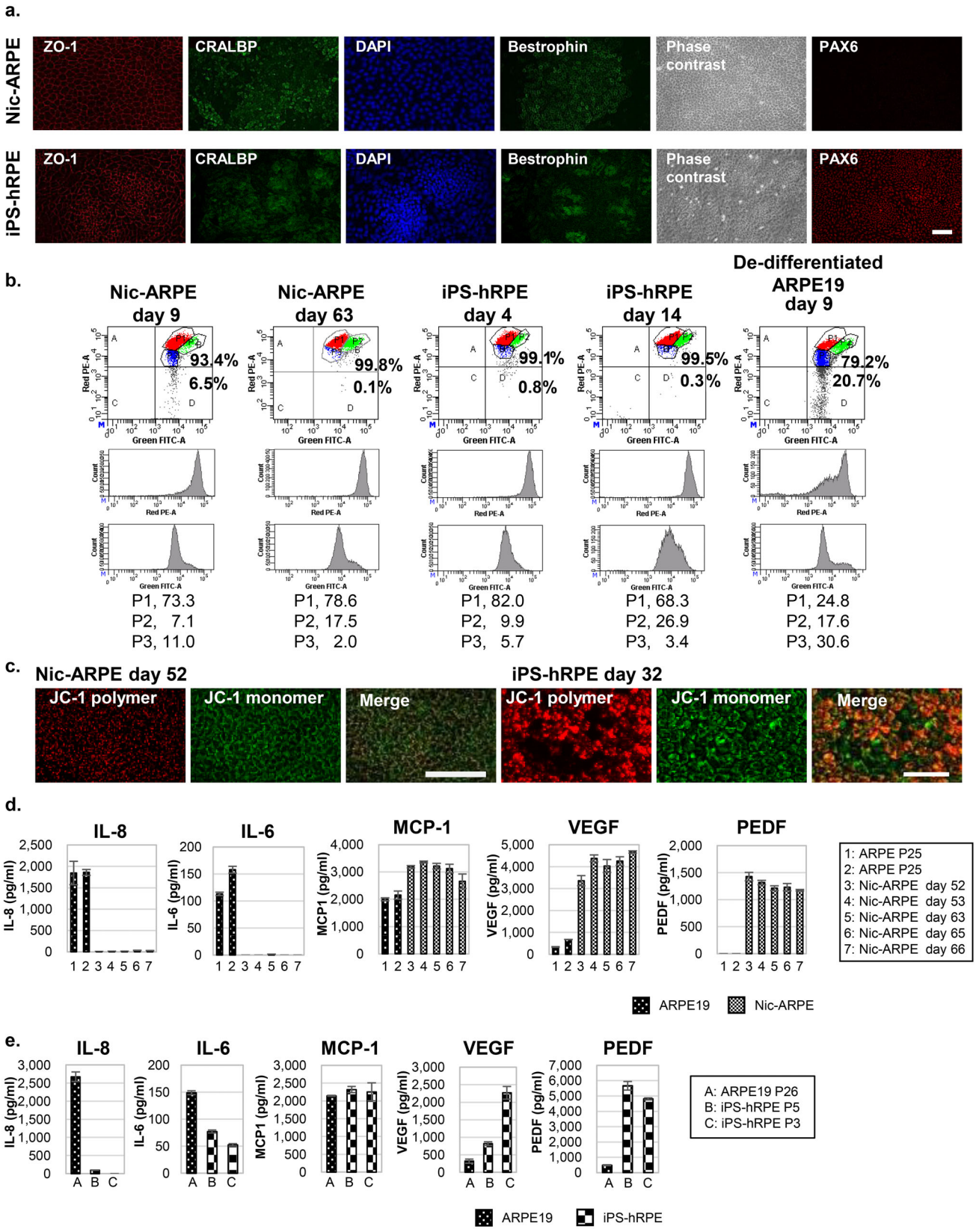

Figure 2. **(a)** Cell phenotypes. ARPE-19 line (P24) cultured for 3 days in DMEM/F12 was reseeded into 48-well culture plates (wp) with a cell density of 6×10^5 cells/ml $\times$ 0.25 ml/well in the presence of NAM (10mM) for 14 days (preculture). Then, the harvested cells were reseeded into 24 wp with a cell density of 5×10^4 cells/ml $\times$ 0.5 ml/well in the presence of NAM (10mM) for 63 days to obtain Nic-ARPE cells (the culture principle the same as shown in Fig. 1). iPS-hRPE cells (P5) were seeded into 24 wp with a cell density of 5×10^5 cells/ml

× 0.5 ml/well and cultured for 14 days. The cell phenotypes were confirmed by phase contrast microscopy and fluorescence microscopy for ZO-1, CRALBP, BEST, and Pax-6. Nic-ARPE cells exhibited a clear cobblestone appearance and were positive for BEST, CRALBP, and ZO-1 in immunostaining (left) but not for Pax-6. iPS-RPE cells were positive for all four of these antigens, including Pax-6 (right). The staining experiments were repeated more than three times to confirm the results. Scale bar: 100 µm. (**b**) Mitochondrial phenotypes. Changes in the mitochondria membrane potential (MMP) were detected with JC-1 dye using the JC-1 Mito MP Detection Kit. The collected cells were incubated with 2 mM JC-1 for 30 min at 37°C and then analyzed with BD FACS Canto II for fluorescence FITC (green) and PE (red). The upper lane shows the dot plot indicating the presence of human (h) RPE cell subpopulations (SPs) distinct in MMP, and the second and third lanes respectively show histograms of green FITC by monomeric JC-1 and red PE fluorescence by aggregated polymeric JC-1. Three SPs, green^{+} and red $^{+++}$ (P1), green^{+++} and red^{+++} (P2), and green^{+} and red^{+} (P3) were detected in gate B. Proportions of subpopulations (SPs) are shown in the lower lanes. Both Nic-ARPE cells at day 9 (namely, P25, 5 × 10^4 cells/mL × 0.5 ml/well in 24 wp) and those after differentiation disposition at day 63 were analyzed. As a control, de-differentiated ARPE19 cells cultured for nine days (P25, 5 × 10^4 cells/mL × 0.5 mL/well in 24 wp) in DMEN/F12 were applied. Both iPS-hRPE cells at day 4 (P5, 5 × 10^5 cells/ml × 0.5 mL/well/24 wp) and those after differentiation disposition at day 14 were analyzed. N = 3 in the staining experiments, and representative pictures are shown. (**c**) Mitochondrial membrane potential. For fluorescence imaging analysis, some hRPE cells shown in Figure 2b were analyzed using a BZ X-700 Microscope System. The morphology of mitochondria in Nic-ARPE and iPS-hRPE cells showed large differences, indicating more enlarged sizes in iPS-hRPE cells. *Scale bar:* 100 and 50 µm for Nic-ARPE and iPS-hRPE cells, respectively. (**d, e**) Production of proinflammatory and angiogenesis-related cytokines. The production of proinflammatory and angiogenesis-related cytokines by Nic-ARPE cells (P27) and de-differentiated ARPE19 cells (P25) (**d**), as well as by de-differentiated ARPE19 cells (P26) and iPS-hRPE cells (P3 or P5) (**e**) were compared. The culture supernatants (CSs) were harvested 48 h after the final medium changes, and ELISA was performed. De-differentiated ARPE19 cells were cultured for three days with a cell density of 0.8 × 10^5 cells/ml × 0.5 mL/well in 24 wp (**d, e**). Nic-ARPE cells were cultured for 52, 53, 63, 65, and 66 days after seeding with a cell density of 1 × 10^5 cells/mL × 0.5 mL in 24 wp (**d**). The iPS-hRPE cells were cultured for 14 days with a cell density of 5 × 10^5 cells/mL × 0.5 ml in 24 wp (**e**). Each column shows the standard deviation bars from four measurements. The experiments were repeated three times independently, and the representative results were presented.

cycle threshold method (2^-ΔCT). The efficiency of transduction of miR-494-3p mimics into ARPE19 and iPS-hRPE cells is depicted (Supplementary Fig. S4). VO-OHpic trihydrate (VO), a pharmacological inhibitor of PTEN, was purchased from Abcam (Cambridge, UK).

Mitochondrial Membrane Potential

Changes in the mitochondrial membrane potential (MMP) were detected using the JC-1 MitoMP Detection Kit (Dojindo Laboratories, Kumamoto, Japan). After the treatment, cells were harvested via Trypsin (Sigma-Aldrich) treatment and suspended at a density of 10^6 cells/mL. The collected cells were incubated with 2 mM JC-1 for 30 minutes at 37°C. After washing with Hanks balanced salt solution, the cells were analyzed using a BD FACS Canto II Flow Cytometry System (BD Biosciences, Franklin Lakes, NJ, USA). For fluorescence imaging analysis, cells were incubated with 2 mM JC-1 for 30 minutes at 37°C and analyzed using a BZ X-700 Microscope System (Keyence). Red stains indicate JC-1 aggregates (dimers) in intact mitochondria, and green stains indicate JC-1 monomers in apoptotic cells with the depolarization of MMP.

Mitochondrial Respiration Assay

The effects of miR-494-3p inhibition on the mitochondrial oxygen consumption rate (OCR) in ARPE-19, Nic-RPE, and iPS-RPE cells were assessed using a Seahorse Bioscience XFe96 analyzer (Agilent Technologies, Santa Clara, CA, USA) in combination with the Seahorse Bioscience XF Cell Mito Stress Test assay kit following the manufacturer's protocol. A real-time metabolic analysis of live cells was performed using the Seahorse XFe24 extracellular flux analyzer (Agilent Technologies). The cultured cells were seeded on an XF24 flux analyzer plate. The Mito stress test was performed according to the manufacturer's protocol. The cell culture medium was replaced one hour before the assay with minimal XF DMEM medium supplemented with 2 mmol/L glutamine, 10 mmol/L glucose, and 1 mmol/L sodium pyruvate (pH 7.4). The OCR was analyzed under basal conditions and after sequential injections of 1 µM oligomycin, 1 µM FCCP, 0.5 µM rotenone, and antimycin. The assay results were normalized on the basis of the viable cell number counted by Cell Insight NXT (Thermo Fisher Scientific).

ATP and NAD$^+$/NADH Assay

The cellular ATP concentration was measured using ATP Assay Kit-Luminescence (Dojindo Laboratories) according to the manufacturer's protocol. Cells were detached using trypsin (Sigma-Aldrich), and 5 × 10^4 cells/mL were used for the ATP assay. The luminescence was measured using GloMax Explorer (Promega Corporation, Madison, WI, USA) according to the manufacturer's instructions. The NAD$^+$/NADH Assay Kit-WST (Dojindo Laboratories) was used to measure the total NAD+/NADH and NADH amounts in hRPE cells according to the manufacturer's instructions. Specifically, 2.5 × 10^5 cells were used for the NAD$^+$/NADH assay. These cells were lysed with NAD/NADH Extraction buffer, spun in a centrifuge at 12,000*g* for five minutes, transferred into the MWCO 10K filtration tube, and centrifuged further at 12,000*g* for 10 minutes. The filtrates (100 µl/tube) were transferred into two 1.5 mL tubes. For disassembling NAD$^+$, one of the tubes was incubated for 60 minutes at 60°C. The samples lysed with NAD/NADH control buffer and the lysates were transferred to a 96-well plate and incubated for 60 minutes at 37°C. The absorbance was measured using iMark microplate reader (Bio-Rad Laboratories, Hercules, CA, USA) at 450 nm.

Western Blotting

The procedures followed those described previously.[32] MagicMark XP Western Protein Standard (Thermo Fisher Scientific) was used as the molecular weight marker. The protein bands were visualized using a Western BLoT HRP substrate series (TakaraBio, Shiga, Japan).

Statistical Analysis

The data are presented as mean ± SD. A statistical analysis of differences was performed using Student's *t*-test for comparisons between two groups. For analysis of variance, this was followed by either Tukey's or Dunnett's test. The values shown in the graphs represent the mean ± SD. In

Investigative Ophthalmology & Visual Science

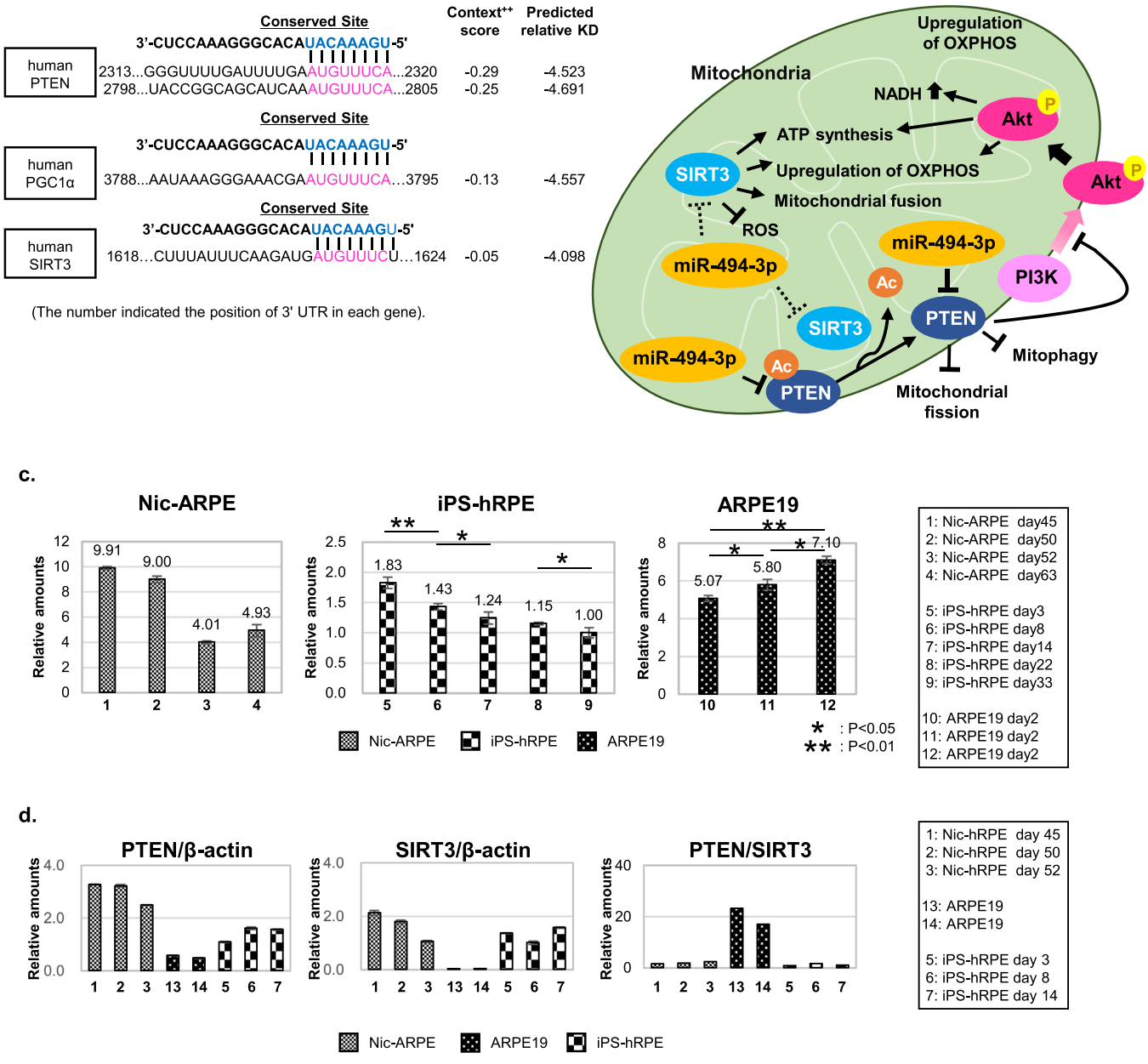

Figure 3. Expression levels of miR-494-3p, its target proteins, PTEN and SIRT3 between Nic- and iPS-hRPE cells. (**a**) Target sites of miR-494-3p. To explore the mechanisms of action of miR-494-3p, Target Scan Human 8.0 (www.targetscan.org) was used to predict the potential targets of miR-494-3p. Among 627 candidates, PTEN, SIRT3, and PGC1α were selected as the potential targets involved in mitochondrial homeostasis. The Kd values of the latter two were far lower than that of PTEN.[33] In addition, the context^{++} score represents the efficacy of repression of the targeting mRNA.[50] PTEN: phosphatase and tensin homolog, SIRT3: sirtuin3, PGC1α: peroxisome proliferators–activated receptor-γ co-activator-1α. (**b**) Illustrated plausible molecular interplays. Inhibition of PI3K/Akt pathway by PTEN. Both activated Akt and SIRT3 serve to enhance mitochondria OXPHOS, ATP synthesis, and NAD^+ elevation. In contrast, PTEN inhibits PI3K-mediated activation of Akt. MiR-494-3p localized in or near mitochondria binds to its target mRNAs and then reduces the expression level in a binding-affinity–dependent manner. PI3K, phosphatidylinositol-3 kinase; Akt, protein kinase B; ATP, adenosine triphosphate; NAD^+, nicotinamide adenine dinucleotide. (**c**) Expression intensity of miR-494-3p, PTEN, and SIRT3. The expression levels of miR-494-3p were quantified by qRT-PCR at the same time by using RNA extracted from the three cultured hRPE cells. Gene expressions were normalized to RNU44 using the comparative cycle threshold method (2ˆ-ΔCT). The relative intensity was expressed by arbitrarily adjusting that of iPS-hRPE (P3, day 33) to 1. The cells tested are as follows: Nic-ARPE cells, days 45, 50, 52, 63 (P27, 24 wp, 5×10^4 cells/mL × 0.5 mL/well), on day 50, cells in the culture were supplemented with N2 instead of N1. De-differentiated ARPE19 cell linesP25, day 2, 12 wp, 8×10^4 cells × 1 mL/well; P26, day 2, 24 wp, 8×10^4 cells/mL × 0.5 mL/well; and P25, day 2, 12 wp, 1×10^5 cells/mL × 1 mL/well and for iPS-hRPE, P5 and P3, 5×10^5 cells/mL × 1 mL/well, 12 wp. Each column shows the standard deviation bars from four measurements. The experiments were repeated three times independently (*$P < 0.05$, **$P < 0.01$). (**d**) Relative expression levels of PTEN and SIRT3. The expression levels of PTEN and SIRT3 were compared by Western blotting and quantified using Image J. The relative expression intensity was calculated against control β-actin. The RPE cells used are the same as those shown in **c**. (**d**) Columns are shown with the standard deviation bars from three measurements. The experiments were repeated three times independently. (*$P < 0.05$, **$P < 0.01$).

Investigative Ophthalmology & Visual Science

all the experiments, the measurements were performed in quadruplicate or triplicate (n = 4 or 3) and three independent experiments were performed (N = 3), unless otherwise stated.

Results

Cell Phenotypes and Culture Conditions

The ARPE-19 line is the most commonly used hRPE cell line. However, after 20 years of passaging, it no longer forms a cobblestone morphology.[24] All the ARPE19 cells used here also showed the de-differentiated (senescent and EMT) phenotypes as exemplified in Supplementary Figure S3. NAM, a form of vitamin B3, participates in metabolic pathways.[30] Although the ARPE-19 line cultured in the presence of NAM continued to differentiate, the ARPE-19 line cultured in the absence of NAM lost the cobblestone appearance and appeared to have undergone de-differentiation.[26,27] In the present study (cultures without Transwell inserts, different from those of Hazim et al.[26,27]), the ARPE-19 line cultured in the presence of NAM in DMEM/F12 was confirmed to differentiation disposed around day 50, and on day 55 to 66, it exhibited a maximally clear cobblestone appearance, as well as positivity for BEST, CRALBP, and ZO-1 (Fig. 2a upper) but not for Pax-6. One type of primary hRPE cells, iPS-RPE cells cultured until five passages showed positivity to all four of these antigens (Fig. 2a lower). Stem-cell-derived RPE cells have been found to lose their polarized organization and RPE functions after only a few passages in culture.[23] Accordingly, in this study, we compared ARPE cells cultured in the presence of NAM (Nic-ARPE cells) and iPS-hRPE cells cultured for three to five passages. The standard methods for the preparation of Nic-ARPE and iPS-hRPE cells are summarized in Figure 1.

Mitochondria Phenotypes and Membrane Potential

The changes in the MMP were detected using the JC-1 Mito MP Detection Kit (Dojin Laboratories). The collected cells were incubated with 2 µM JC-1 for 30 minutes at 37°C. The cells were analyzed using a flow cytometry system (Fig. 2b). The upper lane shows a dot plot indicating the presence of distinct RPE cell subpopulations (SPs) in the MMP, and the second and third lanes, respectively, show histograms of red PE fluorescence by aggregated JC-1 and green FITC by monomeric JC-1. The intensity of the aggregated JC-1dimers was divided into three SPs, two in gate D and one in gate B (Fig. 2b). Continuous NAM addition in ARPE19 cultures in MEM medium induced the disappearance of red PE fluorescence by aggregated JC-1 positive SPs in gate D, indicating the advanced maturation of ARPE19 cells with highly active MMP mitochondria. In the dot plot, three cell SPs -P1, P2, and P3- were distinguished in gate B and were populated with cells showing a strong intensity of both dimeric and monomeric JC-1. Nic-ARPE cells cultured for 63 days clearly showed a decrease in low- to medium-intensity red PE fluorescence, indicating the cell maturation into RPE cells with highly active MMP mitochondria. In this context, iPS-hRPE cells at day 14 showed a red PE fluorescence intensity that was almost the same as that of Nic-ARPE cells at day 63, whereas green FITC fluorescence positive SPs were clearly diminished (indicated by the change in the ratio of P2 SP from 9.9% to 26.9%) during days 4-14 of the culture period (Fig. 2b). Furthermore, for fluorescence imaging analysis, cells were analyzed using a BZ9000 Microscope System (Fig. 2c).

Cell Phenotypes and Culture Conditions

The ARPE-19 line is the most commonly used hRPE cell line. However, after 20 years of passaging, it no longer forms a cobblestone morphology.[24] All the ARPE19 cells here used showed the de-differentiated (senescent and EMT) phenotypes as exemplified in Supplementary Figure S3. NAM, a form of vitamin B3, participates in metabolic pathways.[30] The morphology of mitochondria in Nic-ARPE cells and iPS-hRPE cells showed large differences, with enlarged sizes in the latter, indicating that both RPE cells are not fully identical at least in terms of their mitochondrial morphology.

Production of ProInflammatory and Angiogenesis-Related Cytokines

The production of proinflammatory and angiogenesis-related cytokines by Nic-hRPE cells (P27) and ARPE19 cells (P25) (Fig. 2d), as well as that by ARPE19 cells (P26) and iPS-hRPE cells (P3 or P5) (Fig. 2e) was compared. The CSs were harvested 48 hours after seeding the cells, and ELISA was performed. The production of the proinflammatory cytokines IL-8 and IL-6 was lower in Nic-ARPE and iPS-hRPE cells compared with that in de-differentiated ARPE19 cells, whereas no significant changes were observed for MCP-1 (Fig. 2d). In contrast, the production of both angiogenic VEGF and anti-angiogenic PEDF was higher in the former two hRPE cells.

miR-494-3p/SIRT3/PTEN Axis in Regulating Mitochondria Quality

To further explore the mechanisms underlying the action of miR-494-3p, Target Scan Human 8.0 (www.targetscan.org) was used to predict the potential molecular targets of miR-494-3p. Among 627 candidates, PTEN, SIRT3, and PGC1α were selected as the candidate molecules involved in mitochondrial homeostasis, although the Kd values[33] of the latter two were far lower than that of PTEN (Fig. 3a). Figure 3b illustrates the hypothetical molecular interactions between miR-494-3p and these targets, as well as the inhibition of the PI3K/Akt pathway by PTEN. Both activated Akt and SIRT3 serve to enhance mitochondria oxidative phosphorylation (OXPHOS), ATP synthesis, and NAD^+ synthesis.[34–38] In contrast, PTEN inhibits the PI3K-mediated activation of Akt.[39] MiR-494-3p localized in or near mitochondria binds to its target mRNAs and then reduces the expression level in a binding-affinity-dependent manner (Fig. 3b). Although PGC1α regulates mitochondrial biogenesis, it localizes mainly in the nucleus;[40] thus PGC1α is not shown in Figure 3b. As shown in Supplementary Figure S5, the miR-494-3p mimic was mostly transduced into mitochondria (Supplementary Fig. S5 and Supplementary).

Expression Intensity of miR-494-3p, PTEN, and SIRT3

Nic-ARPE and iPS-hRPE cells exhibited dynamic changes of MMP. To clarify whether the cellular expression of miR-494-3p will also be dynamically up- or downregulated during cell maturation, qRT-PCR was applied to the RNA extracted from Nic-ARPE, iPS-hRPE, and de-differentiated ARPE19

Investigative Ophthalmology & Visual Science

cells for miR-494-3p expression, and the relative intensity was calculated by normalizing that of iPS-hRPE cells (P3 day 33) to 1 (Fig. 3c). To compare the expression levels of SIRT3 and PTEN, the intensity of bands in Western blotting was detected by Image J, and their relative intensity ratios over the control β-actin were shown together with the PTEN/SIRT3 ratio (Fig. 3d). The expression of miR-494-3p was reduced with hRPE cell differentiation disposition, whereas those of PTEN and SIRT3 were elevated. Notably, the PTEN/SIRT3 ratio in de-differentiated ARPE19 cells was around 20 times higher than those in Nic-ARPE and iPS-hRPE cells.

Relative Expression Levels of Mitochondria Proteins

To detect the mitochondrial marker proteins and antioxidative stress markers, qRT-PCR was similarly applied to Nic-ARPE, iPS-hRPE, and de-differentiated ARPE19 cells (TFAM, TOMM20, VDAC1, SIRT3, Nrf2, and PGC1α). The expression

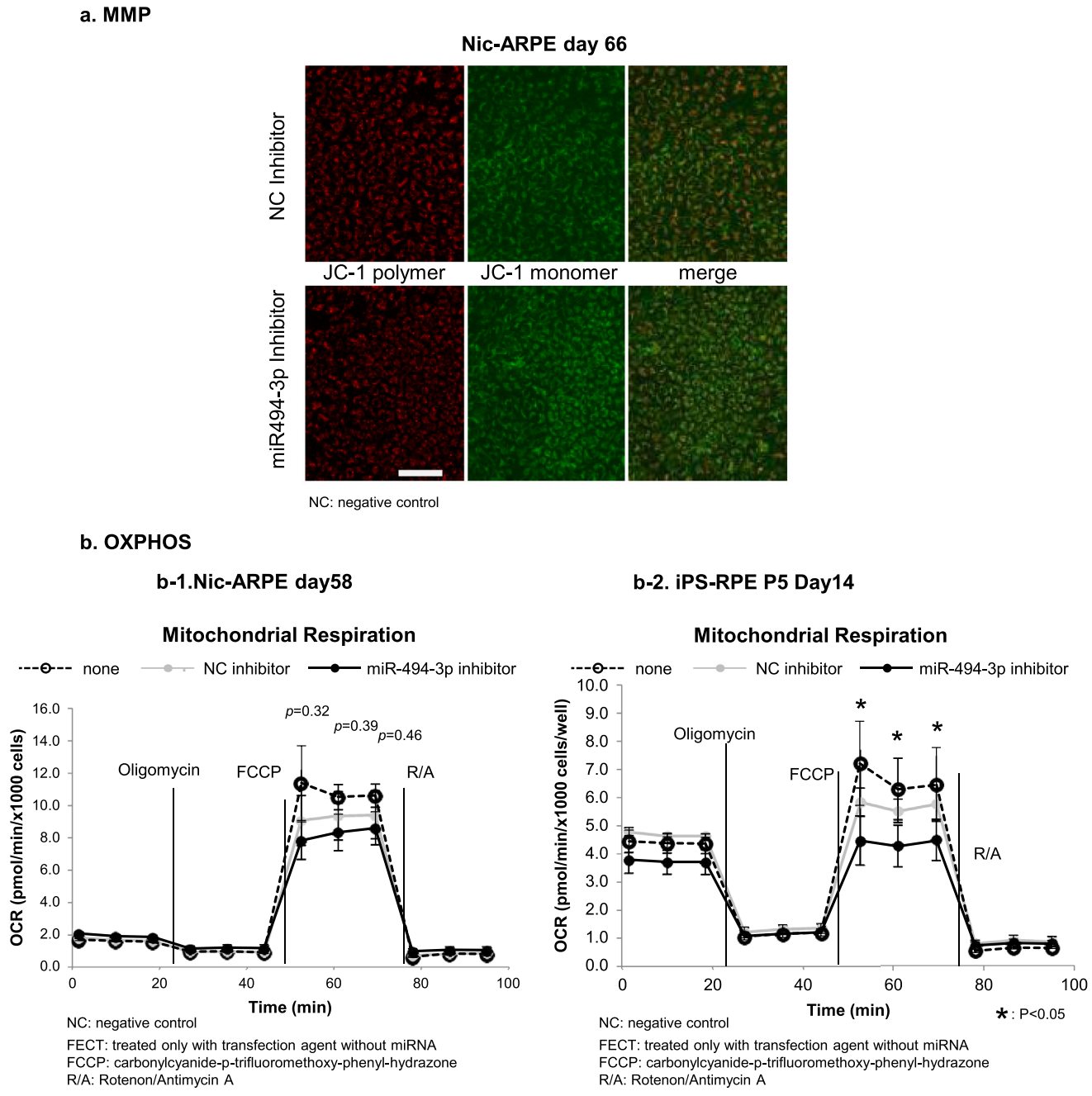

Figure 4. Functional changes of mitochondria by indirect activation of PTEN through inhibition of miR-494-3p by transfection of a miR-494-3p inhibitor. (**a**) Mitochondrial membrane potential (MMP) in Nic-ARPE cells. The MMP was investigated as described in Figure 2c for Nic-ARPE cells (P25, day 66) 48 hours after transfection of a negative control (NC) inhibitor or a miR-494-3p inhibitor. N = 3 in the staining experiments, and representative pictures are shown. *Scale bar:* 100 µm. (**b**) Mitochondrial oxidative respiration (OXPHOS). Mitochondrial OXPHOS was measured using a Mito Stress Test assay kit for the Nic-ARPE cells described above (**b-1**) and for iPS-hRPE cells (P5, day 14) (**b-2**). OCR of 1000 viable cells was expressed. (*$P < 0.05$, N = 4, for Flux analysis). OCR, oxygen consumption rate; FECT, treated only with transfection agent without miRNA; FCCP, carbonylcyanide-p-trifluoromethoxy-phenyl-hydrazone; R/A, Rotenone/Antimycin A.

Investigative Ophthalmology & Visual Science

of mitochondrial markers tended to be elevated in parallel with RPE cell differentiation disposition and the increased expression of SIRT3 and PTEN (Supplementary Fig. S6). The expression of Nrf2 was low in Nic-ARPE cells, thus showing a sharp contrast from the significantly elevated expression in iPS-hRPE cells during the prolonged culture period.

miR-494-3p Inhibitor and Mimic Regulate Mitochondrial Metabolic Homeostasis

A negative control (NC) inhibitor or a miR-494-3p inhibitor was transduced into Nic-ARPE cells (P25, day 64) or iPS-hRPE cells (P5, day 14). The changes in the MMP were analyzed 48 hours after staining (Fig. 4a). A miR-494-3p inhibitor reduced MMP in Nic-ARPE cells. The forced transfection of a miR-494-3p inhibitor into Nic-ARPE cells showed a moderate, but not statistically significant, reduction in the maximum OCR in the Mito Stress Test (Fig. 4b-1). However, forced transfection into iPS-hRPE cells elicited a statistically significant reduction in the OCR (Fig. 4b-2). In keeping with this observation, the forced expression of miR-494-3p mimic into iPS-hRPE cells elicited a statistically significant elevation in the maximum OCR but not in Nic-ARPE cells (data not shown). The miR-494-3p inhibitor may repress the activity of its target miR-494-3p, resulting in the blockade of the PI3K-AKT pathway through PTEN activation and thereby leading to repressed MMP and OXPHOS in Nic-ARPE and iPS-hRPE cells. The mimic may inversely repress PTEN activity, resulting in the activation of PI3K-AKT and OXPHOS.

Regulation of Mitochondrial Metabolism

ATP Production. An NC inhibitor or a miR-494-3p inhibitor was transduced into Nic-ARPE or iPS-hRPE cells (P28, day 58 or P3, day14, respectively). The inhibitor clearly

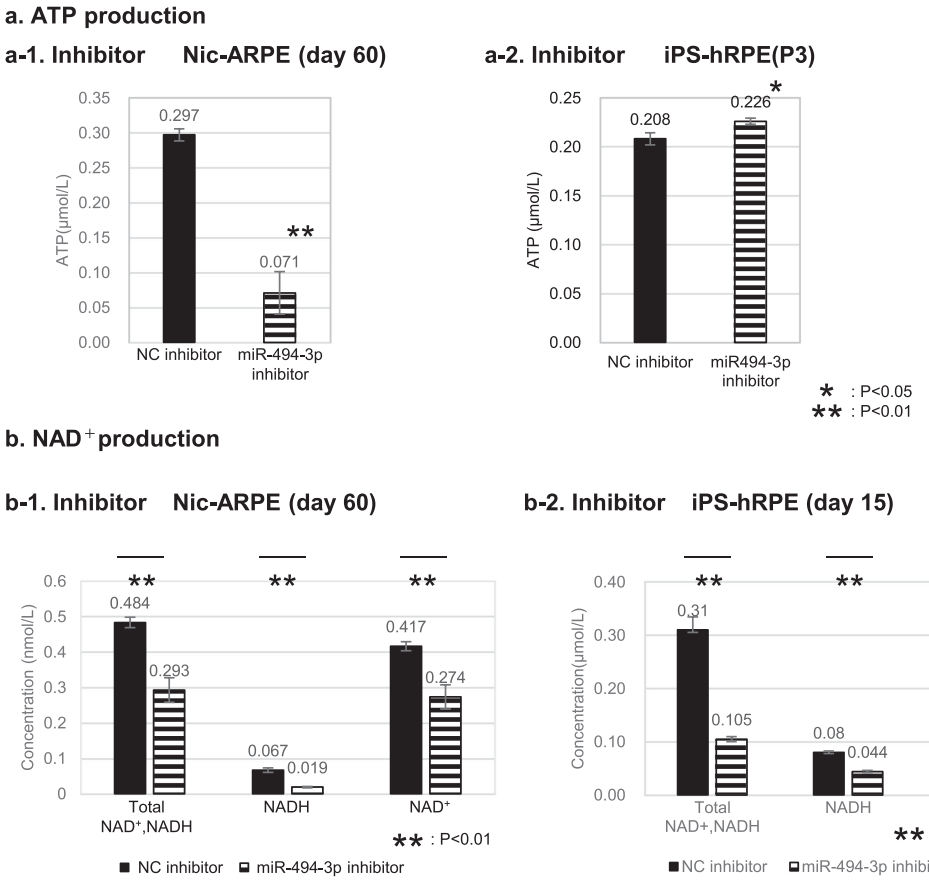

Figure 5. Regulation of mitochondrial metabolism in Nic-ARPE and iPS-hRPE cells. (**a**) ATP synthesis. The cellular ATP concentration was measured using ATP Assay Kit-Luminescence according to the manufacturer's protocol. Cells were detached using trypsin, and 5×10^4 cells/mL were used for the ATP assay. Luminescence was measured using GloMax Explorer (Promega Corporation) according to the manufacturer's instructions (*$P < 0.05$, **$P < 0.01$). Each column shows the standard deviation bars from four measurements. The experiments were repeated three times independently and the representative results were presented. (**a-1)** Inhibitor in Nic-ARPE cells. Nic-ARPE cells (P28, day58) were transfected with a negative control (NC) inhibitor or a miR-494-3p inhibitor and cultured for 48 hours. (**a-2)** Inhibitor in iPS-hRPE cells. The iPS-hRPE (P3, day14) were transfected with an NC inhibitor or a miR-494-3p inhibitor and cultured for 24 hours. (**b**) NAD^+ synthesis. NAD/NADH Assay Kit-WST was used to measure the total NAD^+/NADH and NADH amounts in hRPE cells according to the manufacturer's instructions. The NAD/NADH assay required only 2.5×10^5 cells. The absorbance was measured using an iMark microplate reader at 450 nm. Statistical significances between NCs and an inhibitor were calculated. (**$P < 0.01$, N = 4). (**b-1)** Nic-ARPE cells were produced by culturing ARPE19 cells (P24) with a cell density of 1.5×10^5 cells/well in 48 wp for 14 days (preculture) and then seeding with a cell density of 5×10^4 cells/mL × 0.5 mL/well in 24 wp and cultured in Nic-medium for 60 days. Then, the cells were transfected as described above and cultured for 48 hours. (**b-2) The** iPS-hRPE cells (P5, day 15) were transfected with an NC inhibitor, or a miR-494-3p inhibitor and further cultured for 24 hours.

Investigative Ophthalmology & Visual Science

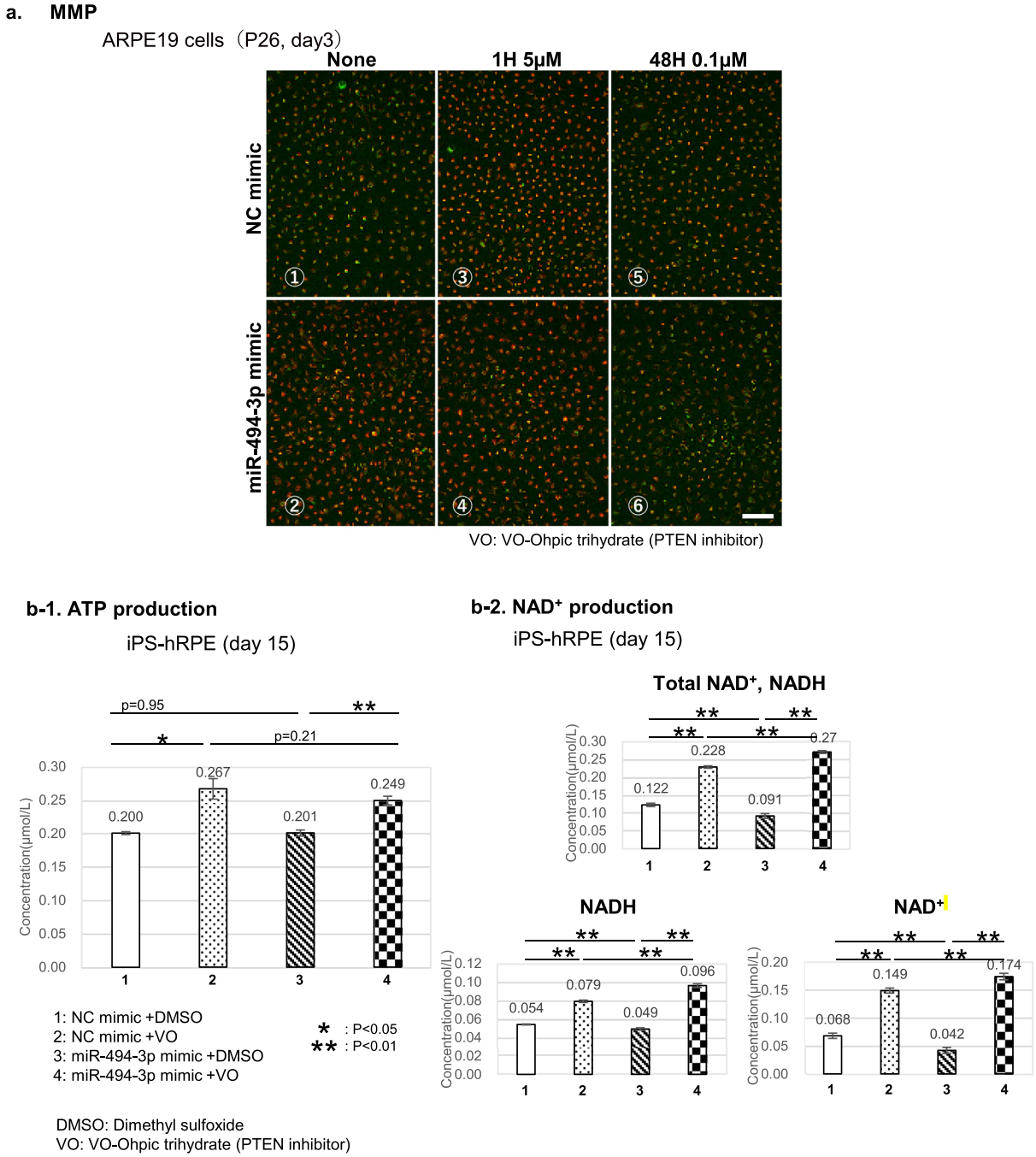

Figure 6. Pharmacological regulation of mitochondrial homeostasis by PTEN inhibitor. (**a**) PTEN inhibitor represses miR-494-3p and elevates MMP in ARPE19 cells. ARPE19 cells (P26) were seeded at a cell density of 4×10^4 cells/mL × 0.5 mL/well in 24 wp. Furthermore, after 24 hours, an NC mimic or a miR-494-3p mimic were transfected, cultured further for 48 hours, and stained with 2 μM JC-1 for 30 minutes at 37°C. VO-Ohpic- trihydrate (VO), a PTEN inhibitor, was added at the same time with the transfection of the mimic. The VO concentration was either 0.1 μM for 48 hours or 5 μM for 1-hour incubation. Experiments were repeated twice. *Scale bar:* 100 μm. (**b**) Elevated ATP and NAD+ production in iPS-RPE. The production of ATP (**b-1**) and NAD^+ (**b-2**) was measured for iPS-hRPE cells (P5, day 15) (*$P < 0.05$, **$P < 0.01$). Each column shows the standard deviation bars from three measurements. The experiments were repeated three times and the representative results were presented.

blocked ATP production through its repression of miR-494-3p activity in Nic-ARPE cells (Fig. 5a-1), whereas a marginal elevation was observed in iPS-hRPE cells (Fig. 5a-2). MiR-494-3p mimic elevated ATP production in these cells through the direct repression of PTEN activity, resulting in the activation of PI3K-AKT. Furthermore, in ARPE cells, the mimic elevated ATP production significantly (Supplementary Fig. S7).

NAD^+ Synthesis. Nic-ARPE cells (P24, day 64) transduced with the miR-494-3p inhibitor exhibited a statistically significant repression of NADH and NAD^+ synthesis (Fig. 5b-1). Similarly, the NC inhibitor or miR-494-3p

inhibitor were transduced into iPS-hRPE cells (P5, day 15). The transduction of the miR-494-3p inhibitor resulted in statistically significant changes of NADH and NAD^+ synthesis (repression) (Fig. 5b-2).

Pharmacological Regulation of Mitochondrial Homeostasis by PTEN Inhibitor

The miR-494-3p mimic directly repressed the PTEN activity, resulting in the activation of PI3K-AKT, whereas the miR-494-3p inhibitor directly repressed the miR-494-3p activity, resulting in the indirect activation of PTEN activity to block the PI3K-AKT pathway. To address this novel regulation of intracellular molecular networks (Fig. 3b), the role of PTEN in mitochondrial homeostasis must be elucidated. To address this issue, we applied VO, a low-molecular-weight pharmacological agent, that can inhibit PTEN activity without cell toxicity against hRPE cells.

In de-differentiated ARPE cells (P26), VO-repressed miR-494-3p elevated MMP. The combined application of both VO and a miR-494-3p mimic elevated MMP in ARPE19 cells (Fig. 6a). The elevation of MMP by a miR-494-3p mimic (①→②) was antagonized by VO (⑤→⑥). Similarly, the elevation of MMP by VO (①→⑤) was also antagonized by a miR-494-3p mimic (②→⑥). The polarizing effects of either VO or miR-494-3p were higher one hour after exposure than they were 48 hours after exposure. No antagonizing effect was observed between VO and miR-494-3p in the elevation of ATP, NAD+, and NADH production in iPS-hRPE cells (Figs. 6b-1, 6b-2). The indirect effect of a miR-494-3p mimic through the repression of PTEN gene expression is not efficient compared with the direct inhibition of PTEN activity by VO. Consequently, VO elicited a more definitive elevation of both ATP and NAD^+ production (Figs. 6b-1, 6b-2).

Discussion

The ARPE19 line has lost the regular cobblestone morphology that is characteristic of differentiated primary hRPE cells after repetitive cell divisions. The ARPE19 cells used in this study for the induction of Nic-ARPE cells showed the characteristics of senescence (owing to repetitive cell division) and EMT, CD44, α-smooth muscle actin, p16, and p21, indicating their inability to address the effect of miR-494-3p on the mitochondrial functions of hRPE cells (Supplementary Fig. S3). The distinction of the expression levels in the characteristics of differentiation/de-differentiation, such as cell morphology, EMT, senescent phenotypes, and SASP production, were evidently confirmed between de-differentiated ARPE19 and Nic-ARPE/iPS-hRPE cells (Figs. 2b, 2d).

The production of IL-8 and IL-6 was lower in Nic-ARPE and iPS-hRPE cells compared with that in degenerated ARPE19 cells, whereas no significant changes were observed for MCP-1 (Fig. 2d). The increased production of proinflammatory cytokines might be ascribed to the senescent features of the latter cells as indicated in Supplementary Figure S3, although it is unclear why MCP-1 production was not elevated in ARPE 19 cells. Considering the differentiation disposed cell features of the former two RPE cells, the elevated production of both angiogenic VEGF and antiangiogenic PEDF is of interest. The regulatory role on angiogenesis might be more specialized role for differentiated RPE cells. Future studies on the polarized production, either apical or basolateral, might be indispensable.

Mitochondrial respiration is one of the reminiscent of the degeneration RPE cells. However, the ways in which the mitochondrial metabolism will be affected by cellular miRs for their cellular functions are not clear. The most interesting finding in the current study is the clear distinction in the expression levels of cellular miR-494-3p, PTEN, SIRT3, and other mitochondrial marker proteins, including PGC1α between differentiation disposed Nic-ARPE cells and iPS-hRPE cells, and de-differentiated ARPE19 cells (Figs. 3c, 3d; Supplementary Fig. S6). The expression profiles of Pax-6 and fine features of MMT (Figs. 2a, 2c) and mitochondrial phenotypes observed by JC-1staining (Fig. 2b) were distinct even between Nic-ARPE cells and iPS-hRPE cells. This may mean that the mitochondrial phenotypes of hRPE cells are plastic, and it may implicate the presence of fragile differentiated phenotypes (Nic-ARPE cells and iPS-hRPE cells) that are reminiscent of the presence of SPs of hRPE cells and in vivo RPE tissues from healthy to an aging or diseased state, such as AMD.

Mitochondria are important organelles that not only generate the majority of cellular energy by OXPHOS but also play important roles in cellular signaling, such as in development and differentiation.[41,42] Figure 3b illustrates the interaction between miR-494-3p and its candidate targets and the inhibition of the PI3K/Akt pathway by PTEN.[43,44] Both activated Akt and SIRT3 serve to enhance mitochondrial OXPHOS, ATP synthesis, and NAD^+ elevation.[34–38] In addition, SIRT3 suppresses the production of reactive oxygen species (ROS) to maintain mitochondrial homeostasis and dynamics.[45] In this context, the expression of Nrf2 was notably marginal even in Nic-ARPE cells, unlike the marked elevation in iPS-hRPE cells, suggesting the presence of antioxidative machinery between both cells.

Although FACS analysis revealed no significant changes in cell SP constitutes by the transfection of a miR-494-3p mimic or inhibitors into iPS-hRPE cells (Supplementary Fig. S8), Mito-tracker Green staining indicated the significant morphological changes in de-differentiated ARPE19 cells when transduced with a miR-494-3p mimic (Supplementary Fig. S9). Precise studies of this issue are essential for better understanding the dynamism of the mitochondrial morphology by enforced transfection to exclude the possibility of transient artificial events.

miR-494-3p localized in or near mitochondria binds to its target mRNAs and then reduces the expression level in a binding-affinity–dependent manner (Fig. 3b). Although PGC1α regulates mitochondrial biogenesis, it mainly localizes in the nucleus.[40] The transcribed mimic and inhibitor were mostly incorporated into mitochondria (Supplementary Fig. S5), making it unlikely for the transduced mimic and inhibitor to encounter PGC1α.

The expression of miR-494-3p is reduced along with disposition of human RPE cell to differentiation (Fig. 3c), whereas the expression of SIRT3 and PTEN was inversely elevated (Fig. 3d). The expression of mitochondrial markers was also elevated along with increased expression of SIRT3 and PTEN. The miR-494-3p inhibitor activates PTEN and blocks the PI3K-AKT pathway, leading to repressed MMP, OXPHOS (Figs. 4a, 4b), and NAD+ production (Figs. 5b-1, 5b-2) in Nic-ARPE cells and iPS-RPE cells. The mimic represses PTEN activity, resulting in the activation of PI3K-AKT, OXPHOS, ATP production, and NAD+ production in iPS-hRPE cells (Supplementary Fig. S7). Hazim et al.[27] recently reported that during NAM-induced differentiation, the mitochondria became larger with more tightly folded

Investigative Ophthalmology & Visual Science

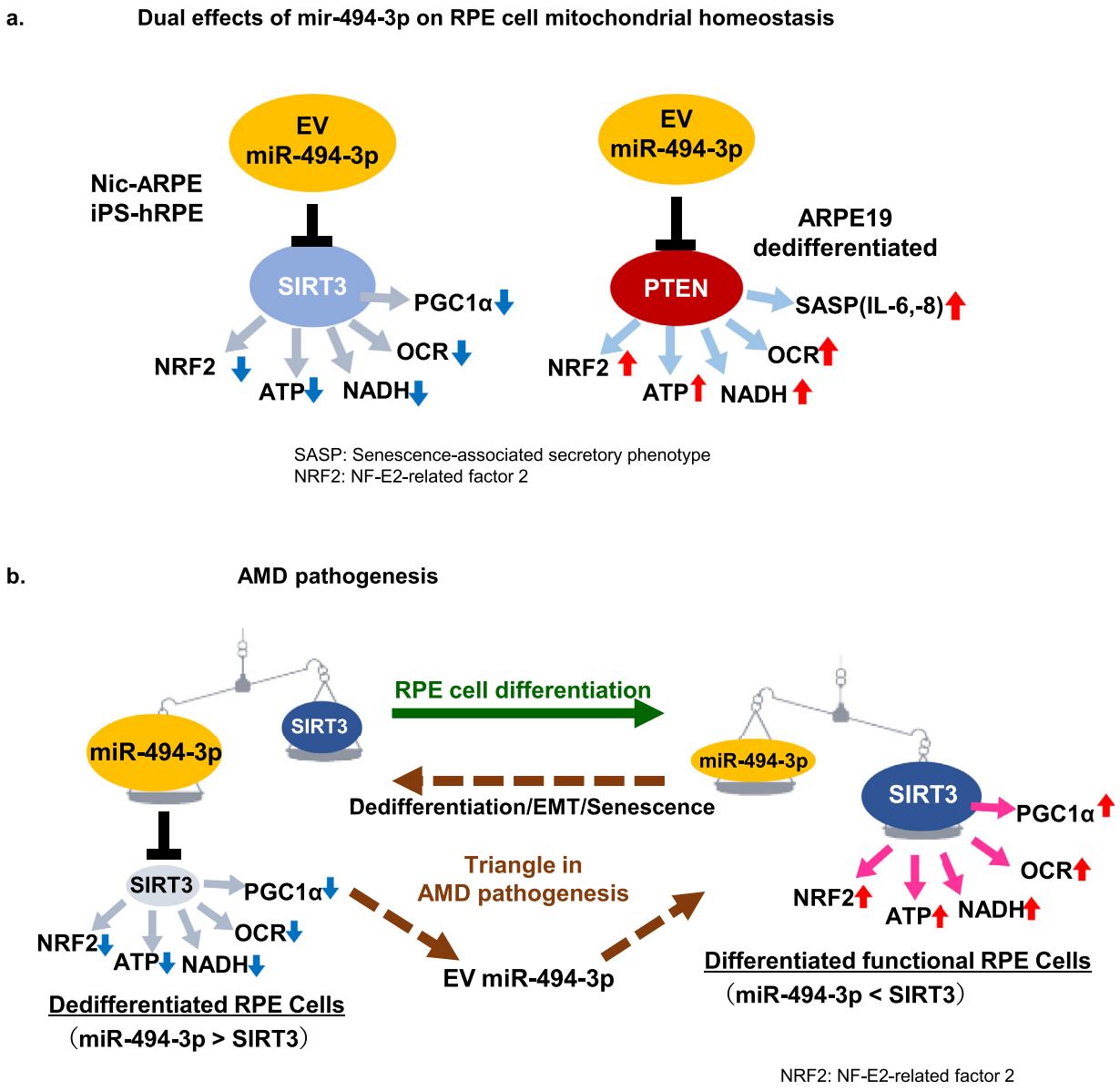

Figure 7. Coordination of human RPE cell quality by miR-494-3p (**a**) Dual effects of miR-494-3p on RPE cell mitochondrial homeostasis. The PTEN versus SIRT3 balance in mitochondria may be critical as one of the causal elements in the degeneration of RPE cells. MiR-494-3p exhibits its dual functions through the interaction either with mitochondria selective SIRT3 or organelle nonselective PTEN. Human RPE cell differentiation will be reprogrammed from de-differentiated RPE (miR-494-3p > SIRT3) to differentiated functional RPE cells (miR-494-3p < SIRT3) along with an enormous change in the intracellular amounts of SIRT3/PTEN. (**b**) Hypothesis of AMD pathogenesis. EV miR-494-3 may induce the spread of degenerated foci in a single-cell layer of RPE tissues (in neighbors). The functional effect will be dependent on the physiological state of the target cell, which influences the competitive interplays between miR-494-3p with PTEN or SIRT3 to coordinate the biogenesis and functional homeostasis of mitochondria of RPE. Accordingly, the proposed interplay among EV miR-494-3p, SIRT3, and PTEN is critical for understanding AMD pathogenesis. In this context, the currently reported results are relevant to understand the homotypic cellular competition among heterogenous RPE cells through EV miR-494-3p as a pivotal molecule in the aggravated degeneration of RPE cells, which may begin in the perifovea and then spread throughout the macula. To claim that these cells are certainly differentiated under the influence of the interaction among miR-494-3p, SIRT3 and PTEN, the claim should be substantiated by experiments with primary RPE cells from fresh tissues.

cristae, and they identified mitochondrial respiration as a key contributor to the differentiated state of the RPE during NAM-induced differentiation. The expression level of PTEN in iPS-hRPE is around half that in Nic-ARPE cells. The expression level of miR-494-3p in iPS-hRPE is around one fifth of that in Nic-ARPE cells. Low levels of miR-494-3p may result in a limited amount of the inhibitor having an efficient impact, indicating the role of cellular miR-494-3p in the differentiation of hRPE cells through the interplay with PTEN (Figs. 3b, 7a). The PTEN inhibitor VO elevated the expression of PGC1α in a manner similar to the miR-494-3p mimic (Supplementary Fig. S10). The indirect effect of the miR-494-3p mimic on PTEN activity through the repression of PTEN gene expression is not efficient when compared with the direct inhibition of PTEN activity by VO (Fig. 6a). VO efficiently elicited the elevation of both ATP and NAD+ produc-

tion compared with miR-494-3p (Fig. 6b), thus supporting the role of PTEN in RPE cell disposition to differentiation (Fig. 7b).

miR-494-3p exhibits its dual functions spatiotemporally through the interplay with either mitochondria selective SIRT3 or organelle nonselective PTEN, which are distributed widely from the nucleus and cytoplasm to the mitochondrial outer membrane. RPE cell differentiation will be reprogrammed from de-differentiated RPE (miR-494-3p > SIRT3) to differentiated functional RPE cells (miR-494-3p < SIRT3) accompanied with a very large change in the SIRT3/PTEN balance, as indicated in Figure 7a. In this context, it is of interest to know whether overexpression of PTEN or inhibition of AKT in ARPE 19 cells will change the morphology and rescue the cells from de-differentiation.

The miR-494-3p versus SIRT3 balance in mitochondria may be critical as one of the causal elements in the degeneration of human RPE cells. EV miR-494-3p elicits paracrine-aggravating effects on the neighboring RPE cell quality. At early AMD, the RPE develops mitochondrial dysfunction, resulting in the cellular heterogeneity of RPE cells; it may begin in the perifovea and then spreads throughout the macula. EV-miR-494-3 may induce spreading into neighbors in single-layer RPE cells from the degenerated foci (Fig. 7b).

The proposed hypothesis for the interplay among EV miR-494-3p, SIRT3, and PTEN is critical for understanding not only the AMD pathogenesis but also the degeneration of RPE cells that constitute a single-cell layer of RPE tissues, as well as for developing novel therapeutic and diagnostic modalities for early AMD. In this regard, the current results show relevant homotypic cellular competition through EV miR-494-3p among heterogenous RPE cells as a pivotal molecule in the aggravated degeneration of RPE cells.

Cellular miR-494-3p has been implicated to be involved in the pathogenesis of various diseases. Specifically, it has been implicated in tissue inflammation, senescence, fibrosis, atherosclerosis, Alzheimer disease, and Parkinson's disease. Notably, the inhibition of miR-494 halts plaque progression and increases plaque stability in mice with established advanced atherosclerotic lesions,[46,47] and the ambient local dynamics appear to share similarities with those in subretinal lesions of AMD.

EV/Exo serve as mediators of crosstalk signaling.[48,49] EV-mediated miR transfer also serves as a signaling mechanism that contributes to the regulation of Mps functions in the subretinal space. Exo are found in RPE cells and in drusen in AMD patients.

Our results demonstrate a clear causal link between miR-494-3p and the degeneration of hRPE cells via the regulation of mitochondrial integrity. Accordingly, elucidating the mechanisms that accelerate RPE cell degeneration is critical not only for understanding AMD pathogenesis but also for developing novel treatment modalities for AMD.

Shortcomings

The present study has revealed partly new interesting findings for future studies. However, it has some shortcomings and unresolved issues. The experimental approach did not use primary human RPE cells from fresh human tissues, and the effects of EVs may well be associated with iPS-derived RPE cells from fresh tissues. Nic-ARPE cells are not primary human RPE cells, and primary hRPE cells, iPS-hRPE cells, may not be identical with the primary cells from fresh tissues. To claim that these cells are certainly differentiated under the influence of the interaction among miR-494-3p, SIRT3, and PTEN, the claim should be substantiated by experiments with primary RPE cells from fresh tissues. The international co-works will be indispensable to use primary RPE cells as a standard for differentiation characteristics. Also, it is quite relevant to know the similar upregulation of PTEN in degenerated RPE tissues compared with innocent tissues. There is no evidence that EV production occurs in vivo by hRPE cells.

Acknowledgments

The authors thank Kazunari Akiyoshi, Satoshi Gojo, Munetoyo Toda, Atsushi Mukai, Eiko Ito, and Takahiro Yamawaki for their assistance during this study and Tomoko Fujita for her technical assistance. The authors also sincerely thank Masayo Takahashi and Helios Co. Inc. for providing the iPS-RPE.

Supported by JSPS KAKENHI Grant Number 20K09807 (J.H.).

Disclosure: **J. Hamuro**, None; **T. Yamashita**, None; **Y. Otsuki**, None; **N. Hiramoto**, None; **M. Adachi**, None; **T. Miyatani**, None; **H. Tanaka**, None; **M. Ueno**, None; **S. Kinoshita**, None; **C. Sotozono**, None

References

1. Evans JR. Risk factors for age-related macular degeneration. *Prog Retin Eye Res.* 2001;20:227–253.
2. de Jong PT. Age-related macular degeneration. *N Engl J Med.* 2006;355:1474–1485.
3. Ambati J, Atkinson JP, Gelfand BD. Immunology of age-related macular degeneration. *Nat Rev Immunol.* 2013;13:438–451.
4. Cherepanoff S, McMenamin P, Gillies MC, Kettle E, Sarks SH. Bruch's membrane and choroidal macrophages in early and advanced age-related macular degeneration. *Br J Ophthalmol.* 2010;94:918–925.
5. Forrester JV. Macrophages eyed in macular degeneration. *Nat Med.* 2003;9:1350–1351.
6. Nussenblatt RB, Lee RW, Chew E, et al. Immune responses in age-related macular degeneration and a possible long-term therapeutic strategy for prevention. *Am J Ophthalmol.* 2014;158:5–11.
7. Yang Y, Liu F, Tang M, et al. Macrophage polarization in experimental and clinical choroidal neovascularization. *Sci Rep.* 2016;6:30933.
8. Cao X, Shen D, Patel MM, et al. Macrophage polarization in the maculae of age-related macular degeneration: A pilot study. *Pathol Int.* 2011;61:528–535.
9. Zandi S, Nakao S, Chun KH, et al. ROCK-isoform-specific polarization of macrophages associated with age-related macular degeneration. *Cell Rep.* 2015;10:1173–1186.
10. Devarajan G, Niven J, Forrester JV, Crane IJ. Retinal pigment epithelial cell apoptosis is influenced by a combination of macrophages and soluble mediators present in age-related macular degeneration. *Curr Eye Res.* 2016;41:1235–1244.
11. Zhou M, Geathers JS, Grillo SL, et al. Role of epithelial-mesenchymal transition in retinal pigment epithelium dysfunction. *Front Cell Dev Biol.* 2020;8:501.
12. Tamiya S, Liu L, Kaplan HJ. Epithelial-mesenchymal transition and proliferation of retinal pigment epithelial cells initiated upon loss of cell-cell contact. *Invest Ophthalmol Vis Sci.* 2010;51:2755–2763.
13. Ghosh S, Shang P, Terasaki H, et al. A role for βA3/A1-crystallin in type 2 EMT of RPE cells occurring in dry age-related macular degeneration. *Invest Ophthalmol Vis Sci.* 2018;59(4):AMD104–AMD113.

14. Wu D, Kanda A, Liu Y, et al. Galectin-1 promotes choroidal neovascularization and subretinal fibrosis mediated via epithelial-mesenchymal transition. *FASEB J.* 2019;33:2498–2513.
15. Hatanaka H, Koizumi N, Okumura N, et al. Epithelial-mesenchymal transition-like phenotypic changes of retinal pigment epithelium induced by TGF-β are prevented by PPAR-γ agonists. *Invest Ophthalmol Vis Sci.* 2012;53:6955–6963.
16. Hatanaka H, Mukai A, Ito E, et al. Epigenetic regulation of the epithelial mesenchymal transition induced by synergistic action of TNF-α and TGF-β in retinal pigment epithelial cells. *Biochem Biophys Res Commun.* 2021;544:31–37.
17. Boles NC, Fernandes M, Swigut T, et al. Epigenomic and transcriptomic changes during human RPE EMT in a stem cell model of epiretinal membrane pathogenesis and prevention by nicotinamide. *Stem Cell Reports.* 2020;14:631–647.
18. Knickelbein JE, Liu B, Arakelyan A, et al. Modulation of immune responses by extracellular vesicles from retinal pigment epithelium. *Invest Ophthalmol Vis Sci.* 2016;57:4101–4107.
19. Jo YJ, Sonoda KH, Oshima Y, et al. Establishment of a new animal model of focal subretinal fibrosis that resembles disciform lesion in advanced age-related macular degeneration. *Invest Ophthalmol Vis Sci.* 2011;52:6089–6095.
20. Yamawaki T, Ito E, Mukai A, et al. The ingenious interactions between macrophages and functionally plastic retinal pigment epithelium cells. *Invest Ophthalmol Vis Sci.* 2016;57:5945–5953.
21. Otsuki Y, Ito E, Mukai A, et al. $CD63^{+}$ extracellular vesicles from retinal pigment epithelial cells participate in crosstalk with macrophages in the innate inflammatory axis. *Exp Eye Res.* 2021;205:108496.
22. Mukai A, Otsuki Y, Ito E, et al. Mitochondrial miRNA494-3p in extracellular vesicles participates in cellular interplay of iPS-Derived human retinal pigment epithelium with macrophages. *Exp Eye Res.* 2021;208:108621.
23. Singh R, Phillips MJ, Kuai D, et al. Functional analysis of serially expanded human iPS cell-derived RPE cultures. *Invest Ophthalmol Vis Sci.* 2013;54:6767–6778.
24. Ahn JY, Datta S, Bandeira E, et al. Release of extracellular vesicle miR-494-3p by ARPE-19 cells with impaired mitochondria. *Biochim Biophys Acta Gen Subj.* 2021;1865(4):129598.
25. Saini JS, Corneo B, Miller JD, et al. Nicotinamide ameliorates disease phenotypes in a human iPSC model of age-related macular degeneration. *Cell Stem Cell.* 2017;20:635–647.
26. Hazim RA, Volland S, Yen A, Burgess BL, Williams DS. Rapid differentiation of the human RPE cell line, ARPE-19, induced by nicotinamide. *Exp Eye Res.* 2019;179:18–24.
27. Hazim RA, Paniagua AE, Tang L, et al. Vitamin B3, nicotinamide, enhances mitochondrial metabolism to promote differentiation of the retinal pigment epithelium. *J Biol Chem.* 2022;298(9):102286.
28. Sugita S, Iwasaki Y, Makabe K, et al. Lack of T cell response to iPSC-derived retinal pigment epithelial cells from HLA homozygous donors. *Stem Cell Reports.* 2016;7:619–634.
29. Sugita S, Kamao H, Iwasaki Y, et al. Inhibition of T-cell activation by retinal pigment epithelial cells derived from induced pluripotent stem cells. *Invest Ophthalmol Vis Sci.* 2015;56:1051–1062.
30. Jang SY, Kang HT, Hwang ES. Nicotinamide-induced mitophagy: Event mediated by high NAD+/NADH ratio and SIRT1 protein activation. *J Biol Chem.* 2012;287:19304–19314.
31. Ueno M, Asada K, Toda M, et al. MicroRNA profiles qualify phenotypic features of cultured human corneal endothelial cells. *Invest Ophthalmol Vis Sci.* 2016;57:5509–5517.
32. Yamashita T, Asada K, Ueno M, et al. Cellular interplay through extracellular vesicle miR-184 alleviates corneal endothelium degeneration. *Ophthalmol Sci.* 2022;2(4):100212.
33. McGeary SE, Lin KS, Shi CY, et al. The biochemical basis of microRNA targeting efficacy. *Science.* 2019;366(6472):eaav1741.
34. Goo CK, Lim HY, Ho QS, et al. PTEN/Akt signaling controls mitochondrial respiratory capacity through 4E-BP1. *PLoS One.* 2012;7(9):e45806.
35. He J, Shangguan X, Zhou W, et al. Glucose limitation activates AMPK coupled SENP1-Sirt3 signalling in mitochondria for T cell memory development. *Nat Commun.* 2021;12(1):4371.
36. Shaik ZP, Fifer EK, Nowak G. Akt activation improves oxidative phosphorylation in renal proximal tubular cells following nephrotoxicant injury. *Am J Physiol Renal Physiol.* 2008;294(2):F423–F432.
37. Kadota T, Yoshioka Y, Fujita Y, et al. Extracellular vesicles from fibroblasts induce epithelial-cell senescence in pulmonary fibrosis. *Am J Respir Cell Mol Biol.* 2020;63:623–636.
38. Dai SH, Chen T, Wang YH, et al. Sirt3 attenuates hydrogen peroxide-induced oxidative stress through the preservation of mitochondrial function in HT22 cells. *Int J Mol Med.* 2014;34:1159–1168.
39. Cantley LC, Neel BG. New insights into tumor suppression: PTEN suppresses tumor formation by restraining the phosphoinositide 3-kinase/AKT pathway. *Proc Natl Acad Sci USA.* 1999;96:4240–4245.
40. Wu Z, Puigserver P, Andersson U, et al. Mechanisms controlling mitochondrial biogenesis and respiration through the thermogenic coactivator PGC-1. *Cell.* 1999;98:115–124.
41. Friedman JR, Nunnari J. Mitochondrial form and function. *Nature.* 2014;505(7483):335–343.
42. Ishihara T, Kohno H, Ishihara N. Physiological roles of mitochondrial fission in cultured cells and mouse development. *Ann N Y Acad Sci.* 2015;1350:77–81.
43. Worby CA, Dixon JE. PTEN. *Annu Rev Biochem.* 2014;83:641–669.
44. Pompura SL, Dominguez-Villar M. The PI3K/AKT signaling pathway in regulatory T-cell development, stability, and function. *J Leukoc Biol.* 2018;103:1065–1076.
45. Someya S, Yu W, Hallows WC, et al. Sirt3 mediates reduction of oxidative damage and prevention of age-related hearing loss under caloric restriction. *Cell.* 2010;143:802–812.
46. van Ingen E, Foks AC, Kröner MJ, et al. Antisense oligonucleotide inhibition of microRNA-494 halts atherosclerotic plaque progression and promotes plaque stabilization. *Mol Ther Nucleic Acids.* 2019;18:638–649.
47. Welten SM, Bastiaansen AJ, de Jong RC, et al. Inhibition of 14q32 MicroRNAs miR-329, miR-487b, miR-494, and miR-495 increases neovascularization and blood flow recovery after ischemia. *Circ Res.* 2014;115:696–708.
48. Baig MS, Roy A, Rajpoot S, et al. Tumor-derived exosomes in the regulation of macrophage polarization. *Inflamm Res.* 2020;69:435–451.
49. Lee H, Abston E, Zhang D, Rai A, Jin Y. Extracellular vesicle: An emerging mediator of intercellular crosstalk in lung inflammation and injury. *Front Immunol.* 2018;9:924.
50. Agarwal V, Bell GW, Nam JW, Bartel DP. Predicting effective microRNA target sites in mammalian mRNAs. *Elife.* 2015;4:e05005.

Investigative Ophthalmology & Visual Science